An MPPT technique for unshaded/shaded photovoltaic array based on transient evolution of series capacitor

An MPPT technique for unshaded/shaded photovoltaic array based on transient evolution of series capacitor

R. Ahmad [a,*], Ali F. Murtaza [a], Umar Tabrez Shami [b], Zulqarnain [a], Filippo Spertino [c]

[a] Faculty of Engineering, University of Central Punjab, Lahore, Pakistan
[b] Department of Electrical Engineering, University of Engineering & Technology, Lahore, Pakistan
[c] Energy Engineering Department, Politecnico di Torino, Torino, Italy

Keywords:
I-V curve tracer
Transient evolution of capacitor
Partial shading effects
Photovoltaic (PV) systems

A B S T R A C T

For maximum power point (MPP) application, the transient evolution of capacitor can be exploited to examine the power-voltage (P-V) characteristics of a photovoltaic (PV) array. This method is simple and inexpensive. In addition, it can be implemented on any array size whether un-shaded or partially shaded. This paper presents a new MPPT technique that scans the P-V curve of PV array with a series capacitor (C_{scan}) through a unique H-bridge architecture. The proposed technique employs a simple algorithm, which controls the H-bridge to scan the P-V curve in two sequences: (1) during charging of capacitor, and (2) during discharging of capacitor. The proposed MPPT neither requires the isolation of PV array from load nor executes power loss during checking of P-V curve. The effects of input capacitor (C_{in}) of converter during scanning of P-V curve are comprehensively discussed, and then the correct sizing of C_{scan} according to array size is explained with a design example. A comparative analysis of different MPPTs in the context of tracking ability, dynamic, and steady state efficiencies is presented. This analysis highlights the advantage of proposed technique over other MPPTs. Finally, the fundamental operation of proposed MPPT is verified through experimental results.

1. Introduction

The enormous expansion of photovoltaic (PV) plants around the continents signifies their importance as one of the most popular renewable energy sources (González et al., 2016; Bizon, 2016). Usually, the economic viability of PV plants is estimated based on assumption that PV array will operate in a maximum power point (MPP) region. Since the current - voltage (I-V) characteristics (together with MPP) of PV array fluctuate non-linearly with changing irradiance and temperature (Spertino et al., 2015; Wang et al., 2016; Subudhi and Pradhan, 2013), an inefficient maximum power point tracking (MPPT) technique cannot guarantee optimal operation of PV array. These circumstances can correspondingly have negative ramifications for the overall revenue and expenditure.

In order to harness maximum power from PV arrays, researchers opted low complex MPPTs such as: optimized perturb and observe (P&O) (Femia et al., 2005), adaptive P&O (Piegari and Rizzo, 2009), and variable step size incremental conductance method (Liu et al., 2008). The aforementioned techniques performed moderately in terms of convergence speed; however, these methods wavered in fast varying weather conditions. To improve the performance, numerous MPPT designers proposed hybrid combination of conventional techniques (Sher et al., 2015; Murtaza et al., 2014a; Moradi and Reisi, 2011). Other researchers employed the advanced intelligent algorithms, including fuzzy logic (Chen et al., 2016), and particle swarm optimization (PSO) Chao, 2014. For uniformly irradiated arrays, hybrid and advanced techniques exhibit satisfactory performance; but these MPPTs may falter to track the global maxima (GM) under partial shading condition. The power loss can go up to 70% (Petrone et al., 2008), when MPPT is trapped in the local maxima (LM). During partial shading, multiple local maximum (LMs) appear on P-V curve of the PV array due to activation of bypass diodes (Murtaza et al., 2014b; Seyedmahmoudian et al., 2015). These bypass diodes are connected across the group of series cells, in a PV module, to avoid hot-spot effects.

Under these circumstances, the MPPT developers proposed distinct strategies. Re-configurable MPPTs vary the interconnection between PV modules to decrease the unfavorable effects of partial shading (Bidram et al., 2012). However, the extra cost of semiconductor devices and administration of switching matrix are main drawbacks of this strategy. Circuit topology based MPPTs while providing relief against shading effects require additional

* Corresponding author.
E-mail address: rana.riaz@ucp.edu.pk (R. Ahmad).

sub-systems like module integrated MPPTs, DC- DC converters, multiple inverters, capacitors, multiple switches and sensors (Bidram et al., 2012). Not only the overall cost of the MPPT implementation is high, control is also difficult. MPPTs based on study of characteristics of PV array provide the solution with no additional hardware (Patel and Agarwal, 2008). In search of GM, the technique introduced in Kouchaki et al. (2013) scans the P-V curve with multiple integrals of $0.8V_{oc}$. A better technique is presented in Boztepe et al. (2014), which first restricts the voltage zone of P-V curve and then pursues the GM in that zone. Extended time required by these MPPTs to reach the MPP curtails the energy production considerably. Soft computing based MPPTs revolve around the artificial intelligence concepts, including artificial neural network (Punitha et al., 2013), cuckoo search scheme (Ahmed and Salam, 2014), and wolf optimization process (Mohanty et al., 2015). Optimization procedures involving tuning of multiple parameters and advanced embedded systems are the negative aspects of these MPPTs.

A large portion of aforementioned MPPTs uses the scheme shown in Fig. 1(a), where the duty cycle (D) of the DC-DC converter is used as a control variable to regulate the operating voltage (V_{pv}) or current (I_{pv}). For each perturbation in D, the second order transient of the converter requires execution time in milliseconds (5–50 ms) (Femia et al., 2005; Ortiz-Valencia and Ramos-Paja, 2015) as shown in Fig. 1(b). At times, multiple adjustments in D are required to settle the PV array (V_{pv}) at reference point. Since MPPTs assess multiple points on P-V curve to identify the MPP/GM, the execution time of these MPPTs is in hundreds of milliseconds, if not in seconds. Moreover, the array is not operated at maximum power during the search.

First-order capacitor based MPPTs are suggested in literature (Spertino et al., 2015; Parlak, 2014) for fast scanning that exploits capacitor transients to trace P-V curve. To implement this method, a modification in the conventional circuit is needed as shown by black dotted lines in Fig. 1(a). Using innate characteristics of capacitor, the P-V curve can be scanned in tens of milliseconds. This duration is almost equivalent to the execution time of single voltage step of above mentioned MPPTs as evident in Fig. 1(b) and (c). As a result, capacitor scanning based MPPT has fast convergence speed and better dynamic efficiencies. However, the isolation of PV array from load is required to scan the P-V curve with parallel capacitor (Spertino et al., 2015; Parlak, 2014). Moreover, to re-initialize every subsequent scanning, energy stored previously in the capacitor is dissipated through the external resistor (Spertino et al., 2015). On similar lines, the methods presented in Kotti and Shireen (2015) and Kotti and Shireen (2013) performed the scanning of I-V curve through DC-DC converter. Although these methods use the input capacitor (C_{in}) of converter instead of separate capacitor, they may have compatibility issues with PV arrays having small C_{in}. Note that C_{in} is designed keeping in view the converter design and PV array. In addition, these MPPT consumed extra time to set the converter at one extreme before initializing the scanning. Apart from MPPT, another significant application of this mechanism is the parametric characterization of PV arrays. The P-V curve of array can be traced with the low cost capacitor charging method (Munoz et al., 2011) instead of expensive electronic load as per the described standards (Standard IEC 62446, 2009).

To date, there has been no formal study, which exploits the employment of capacitor in series to scan the P-V curve of array either for MPP application or for parametric characterization. This paper presents a new MPPT to scan the P-V curve with a series capacitor (C_{scan}). Through unique H-bridge architecture, the proposed algorithm traces P-V curve in two sequences: one during transient evolution of charging, and the other during transient progress of discharging of capacitor. With this scheme, the advantages gained are: (1) fast scanning process without isolation of PV array from load, (2) the energy stored in capacitor during charging is re-injected to the load during discharging, and (3) the technique is simple to implement and scalable to any array size. A comprehensive criterion is presented for the accurate sizing of capacitor according to array size and input capacitor (C_{in}) of converter. For comparative analysis, the proposed and previous MPPTs are implemented in Matlab/Simulink and their efficiencies are assessed. Finally, the working principle of proposed MPPT is verified experimentally.

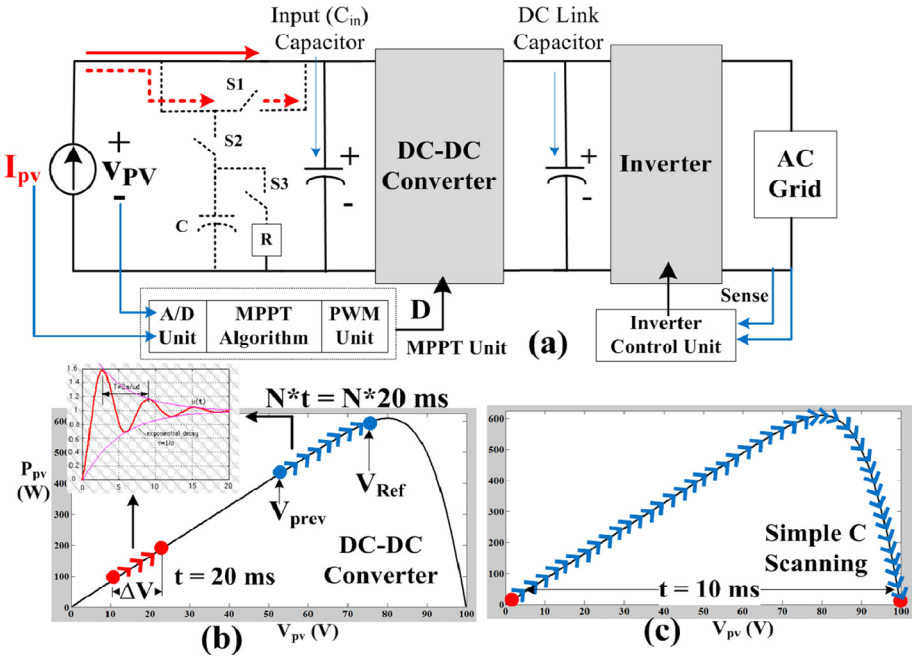

Fig. 1. (a) Basic setup to implement MPPTs (capacitor MPPT circuit in dotted lines), (b) MPPTs execution with DC-DC converter, and (c) Scanning of P-V curve with capacitor.

2. Behavior of PV array with capacitor in series

The capacitor in its transient evolution acts as a variable resistor, which can be used to trace the P-V curve from short-circuit current (I_{sc}) to open-circuit voltage (V_{oc}). Fig. 2(a) presents the I-V curve of PV array from short-circuit current (I_{sc}) to open-circuit voltage (V_{oc}) that is superimposed over the intrinsic characteristics of capacitor. Since PV array is pre-dominantly a current source, its voltage can be varied from 0 to open-circuit voltage (V_{oc}) with series capacitor provided the voltage is maintained at the output as shown in Fig. 2(b). In that case, the transient progress of PV array with capacitor in series is precisely the match of PV array with capacitor in parallel, and no isolation from load is required. However, the regulation of output voltage is needed, which is explained in the next section.

Consider a fully discharged capacitor connected in series with a PV array against the constant DC voltage (V_{dc}) as shown in Fig. 2(b). In such a configuration, the voltage (v_{PV}) of array cannot change instantaneously as capacitor opposes it. With time, the v_{PV} of PV array rises along with v_C until the combination of both becomes equal to constant V_{dc}. The behavior of this configuration from initial time t = 0 to final time t = t_f can be mathematically represented as:

$$v_{PV}(t=0) - v_C(t=0) = V_{dc} \tag{1}$$

$$v_{PV}(t=t_f) - v_C(t=t_f) = V_{dc} \tag{2}$$

By subtracting (2) from (1):

$$\Delta v_{PV} = \Delta v_C = \frac{I_{pv}}{C_{scan}}\Delta t \tag{3}$$

From (3), it can be evaluated that the transient evolution of capacitor's voltage with time (Δt) depends on the current (I_{pv}) of PV array and capacitance of the capacitor. The proposed MPPT adopts this scheme to trace the P-V curve.

3. Designing of MPPT technique

3.1. Basic algorithm

Proposed algorithm works in two simple sequences, where each sequence is executed in four steps. To detect MPP, the first sequence involves tracing of P-V curve by charging the capacitor (C_{scan}); and the second sequence involves scanning by discharging the capacitor (C_{scan}). Note that at a given weather condition, the algorithm processes only one sequence at a time to trace the P-V curve. The other sequence is used for next scanning process whenever weather condition changes.

3.2. H-Bridge architecture & working principle of technique

Fig. 3(a) illustrates the circuit configuration of proposed technique, where the H-bridge contains four switches (S1, S2, S3 & S4) with C_{scan} in between the switches. Consider Sequence-1 (capacitor charging sequence) of technique with a completely discharged capacitor.

Step-1: In start, the pulse width modulation (PWM) unit of proposed technique settles V_{pv} of array at $0.1V_{oc}$ by modulating the D of converter. Initial value of V_{oc} is calculated from the manufacturer's datasheet.
Step-2: After that D is maintained at the same value, and switches S2 and S4 are closed. Consequently, the capacitor (C_{scan}) is hooked up in opposite polarity to PV array as appeared in Fig. 3(b). The mathematical representation of such a circuit is expressed as:

$$v_{PV}(t) \uparrow - v_C(t) \uparrow = 0.1V_{oc} \tag{4}$$

Since $v_C = 0$ at t = 0, PV array starts operating at $0.1V_{oc}$ as indicated by (4) and Fig. 4(a). With passage of time, the capacitor will charge with I_{pv} of array and its v_C rises from zero. This, in turn, causes v_{PV} to rise since the difference between v_{PV} and v_C is equal to the fixed output voltage of $0.1V_{oc}$ as depicted by (4). It should be noted that v_{PV} of array is always above the v_C by $0.1V_{oc}$. Finally, when v_{PV} becomes equal to V_{oc}, v_C reaches $0.9V_{oc}$. In this way, P-V curve is traced from $0.1V_{oc}$ to V_{oc}. This principle is elaborated in Fig. 4(a). During scanning, the MPPT controller keeps on sampling I_{pv} and V_{pv} of array through its analog to digital (A/D) converter as shown in Fig. 3(a). MPPT stores the maximum power (P_{mpp}) and voltage (V_{mpp}) via peak detection sub-routines. To terminate the scanning process, the proposed MPPT controller senses I_{pv} value. The moment I_{pv} becomes equal to zero i.e., $v_{PV} = V_{oc}$, the scanning process is stopped; and the practical V_{oc} value is updated for future processing. With this procedure, the P-V curve is scanned without disconnecting the PV array from load. Since duration of P-V curve scanning depends upon the transient evolution of C_{scan}, the correct sizing of C_{scan} is essential. This is explained in next section.

Step-3: After the initial scanning, switches S3 and S4 are closed to bypass the series capacitor as shown in Fig. 3(d). Thereafter, the PWM unit of MPPT controller varies D to set array at V_{mpp} (stored during the P-V curve scan).
Step-4: A change in weather may occur in 15–25 s during normal conditions (Bekker and Beukes, 2004), whereas this duration is reduced down to a few seconds during windy and cloudy days. Thus, for higher efficiency, it is important to stick to MPP when conditions are steady and to avoid frequent tracing of I-V curve during fast varying weather conditions. To deal

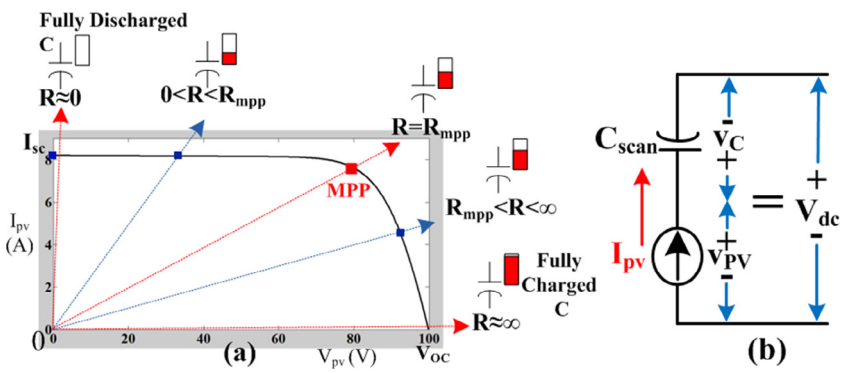

Fig. 2. (a) Capacitor charging with I-V curve, (b) PV array with series capacitor.

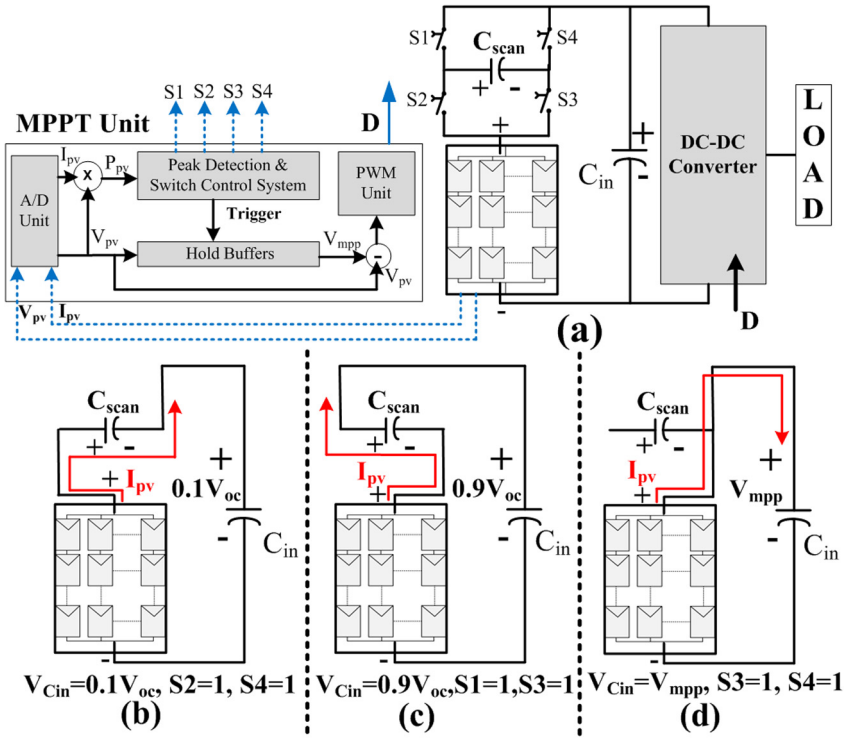

Fig. 3. (a) A H-bridge architecture of proposed MPPT, (b) configuration of circuit with switches S2 and S4 are on, (c) configuration of circuit with switches S1 and S3 are on, and (d) bypass the C_{scan} with S1 and S2 are on.

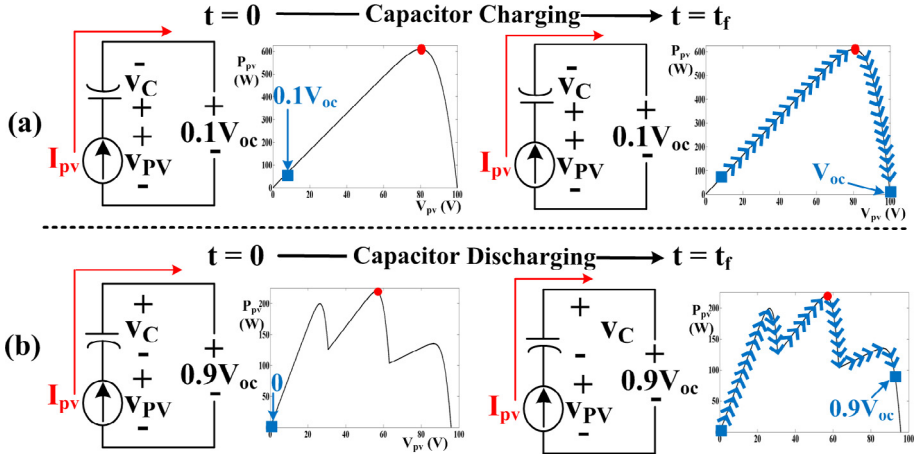

Fig. 4. (a) Tracing of P-V curve (uniformly irradiated PV array) with transient evolution of charging capacitor and (b) Tracing of P-V curve (partially shaded PV array) with transient progress of discharging capacitor.

with such a challenge, the decision to revoke new scanning process is based on two parameters: ±3% P_{mpp} and t_{limit} of 1 min. Fig. 5 displays the working flowchart of this mechanism. Initially, the timer is triggered and power condition is checked whether instantaneous P_{pv} is within ±3% of P_{mpp}. When condition is violated, the timer state is examined. If timer is less than one minute, the algorithm declares it as a fast varying weather and sets the Flag before moving to next scanning. After scanning, timer is reset and triggered again. Consider power of array changes again in less than one minute (timer < 1 min), but this time algorithm will not move to next Sequence since Flag is set during previous iteration as shown in Fig. 5. As a result, the algorithm will wait for remaining time, and then eventually move to next scanning after clearing the Flag.

For slow varying weather conditions, the timer is usually greater than 1 min. In that case, the Flag condition becomes irrelevant, and the proposed method only revokes the new scanning whenever there is a change in power due to variation in weather.

In this research work, the power limit is set at ±3%, which can be optimized further based on the sensing equipment. For instance, the sensing limit can be reduced further through sophisticated instrument. On the other hand, t_{limit} is related to weather condition, the nature of which is difficult to predict. Consequently, t_{limit} is calibrated based on the simple assumption that once I-V curve is scanned, the process should not be repeated for at least 1000 times of scanning duration. Nevertheless, the historical meteorological data of a specific location can be consulted to optimize the t_{limit} further.

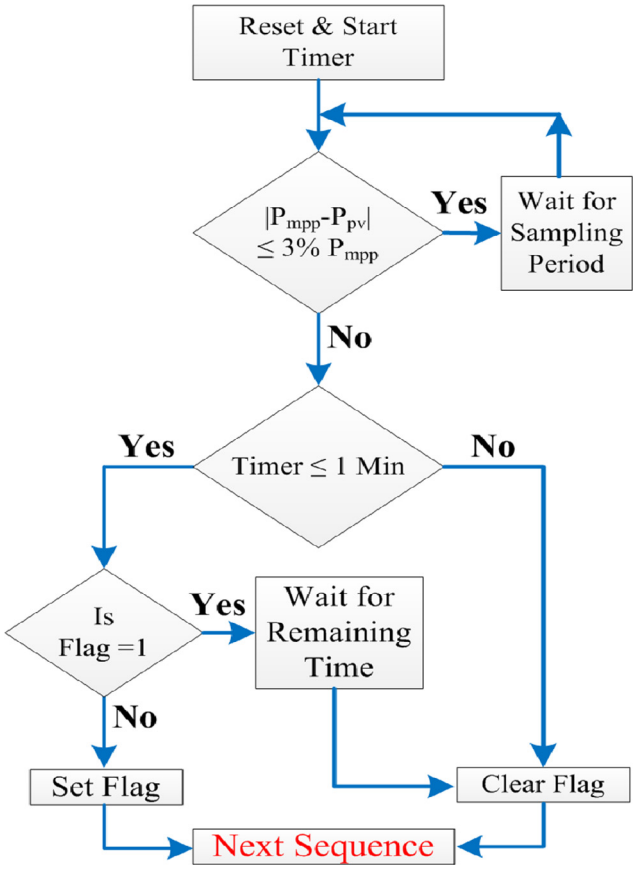

Fig. 5. Power condition and timer based mechanism to revoke new scanning.

In Sequence-2 (capacitor discharging sequence), the proposed MPPT executes the following four steps:

Step-1: In the start, MPPT controller of proposed method adjusts D to set the PV array at $0.9V_{oc}$.
Step-2: S1 and S3 switches are turned on. The circuit takes the configuration where both PV array and capacitor (C_{scan}) are connected in series with the same polarity as shown in Fig. 3(c). This can be mathematically expressed as:

$$v_{PV}(t) \uparrow + v_C(t) \downarrow = 0.9V_{oc} \tag{5}$$

Note that C_{scan} is already charged to $0.9V_{oc}$ during the previous iteration in Sequence-1. Since the output voltage is fixed at $0.9V_{oc}$, v_{PV} is zero at t = 0 as depicted by (5). This mechanism is presented in Fig. 4(b), where the P-V curve exhibits multiple local maximum (LMs) due to partial shading. With time, the capacitor starts discharging with the rate determined by I_{pv} of array. As a result, v_C of C_{scan} falls while v_{PV} of array rises as indicated by (5). This process continues until C_{scan} becomes completely discharged. At this point, v_{PV} becomes equal to $0.9V_{oc}$ and P-V curve is scanned from 0 to $0.9V_{oc}$ as illustrated in Fig. 4(b). Unlike previous sequence, the proposed MPPT evaluates V_{pv} value to terminate tracing process in the present sequence. When V_{pv} becomes equal to $0.9V_{oc}$, MPPT controller stops the scanning process. The transient evolution of C_{scan} during discharging allows the proposed MPPT to scan the P-V curve and stores MPP parameters. Note that energy stored in C_{scan} during the previous scanning is re-injected into load during the current scanning. Consequently, ideally no energy is wasted. However, during partial shading the scanning duration is prolonged as overall average I_{pv} is low.

Step-3: After scanning, the switches S3 and S4 are switched on as shown in Fig. 3(d), and MPPT controller once again varies the D to bring V_{pv} at V_{mpp}.
Step-4: Follow the same mechanism as shown in flowchart of Fig. 5.

Note that the charging/discharging of C_{scan} depends on I_{pv} of array, which in turn depends on the weather condition. Therefore, the duration to scan P-V curve can be varied from one condition to another. However, the proposed MPPT remains undisturbed as its scanning process is not operated with fixed time. Instead, the duration of scanning process is determined by feedback value of I_{pv} ($\approx$0) in Sequence-1, and feedback value of V_{pv} ($\approx 0.9V_{oc}$) in Sequence-2 as already described. With this working principle, the advantage of proposed MPPT is expected to be prominent over fixed-time scanning algorithm when conditions hover around STC. With PV array operating at low I_{pv} values, the scanning duration of proposed MPPT becomes prolonged, thus reducing its advantage.

4. Effects of C_{in} on I-V curve scan and sizing of C_{scan} value

Fig. 6 displays the innate characteristics of typical PV module and transient evolution of capacitor's charging. To evaluate the time required by the capacitor, consider zone-1 from I_{sc} to MPP. In this zone, PV generator can be approximated as a constant current source. Therefore, the capacitor's voltage (v_C) rises with a constant slope and it will take time (t_o) to reach the MPP voltage (Spertino et al., 2015). While in zone-2 i.e. from MPP to V_{oc} point, the PV generator behaves like a voltage source. In this zone, the capacitor will follow the transient based on RC time-constant (τ). Thus, the time to reach from MPP to V_{oc} point is 5τ (Spertino et al., 2015). As a result, the final time (t_f) to trace the I-V curve is $t_f = t_0 + 5\tau$. The work presented in Mahmoud (2006) has theoretically estimated the relationship between C_{scan} and t_f as indicated in (6), while its experimental validation is presented in Spertino et al. (2015).

$$C_{scan} \cong 0.55 \times \frac{I_{sc,m} \times N_p}{V_{oc,m} \times N_s} \times t_f \tag{6}$$

where N_p and N_S represent the number of modules in parallel and series, respectively. $I_{sc,m}$ and $V_{oc,m}$ correspond to short-circuit current and open-circuit voltage of the module, respectively.

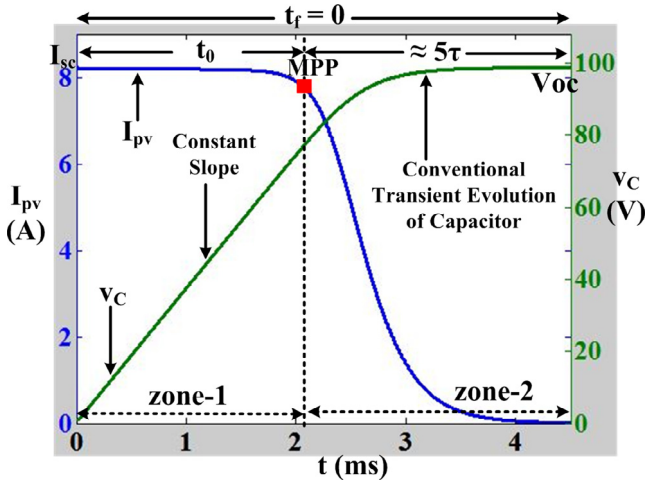

Fig. 6. Transients of capacitor with I-V curve of module.

A comprehensive study is presented in Xiao et al. (2007) to determine the size of input capacitor (C_{in}). According to which, C_{in} of boost converter can be calculated from (7) as:

$$C_{in} = \frac{\Delta i_L}{8 \times \Delta v_{PV} \times f_{sw}} = \frac{10\% I_{mpp}}{8 \times 0.5\% V_{mpp} \times f_{sw}} \quad (7)$$

An experimental test bench is developed according to the setup shown in Fig. 3(a). The details of experimental setup along with labels of devices are mentioned in Fig. 7. PV array consists of six modules, which are organized in 2×3 serial-parallel architecture. Each module has the following ratings at STC condition: I_{sc} = 1.21 A, I_{mpp} = 1.16 A, V_{oc} = 22 V and V_{mpp} = 17.6 V. Boost converter is employed as a power interface circuit between PV array and battery load of 48 V. The L and C_{out} of converter is set at 424 μH and 330 μF, respectively. The switching frequency of converter is set at 35 kHz. Four solid-state relays are used to create an H-bridge.

Using STC data, the C_{in} of PV array comes out as ≈10 μF from (7). Numerous tests have been conducted to scan the I-V curves with distinct C_{scan} capacitors and C_{in} = 10 μF. The details of some tests are indicated in Table 1, where it is separated between two sections: Sequence-1, and Sequence-2. As shown in Sequence-1, the theoretical final time (t_f) values (calculated from (6)) of different C_{scan} capacitors show good resemblance to experimental t_f values. Nevertheless, the scanning duration of proposed technique is based on sensing feedback, which takes care of time variations. The real concern is the voltage drop (ΔV_{Cin}) of C_{in} during this sequence, which in turn disturbs the output voltage. Upper graphs of Fig. 8 display the tracings of I-V curves with C_{scan} of 100 μF, 470 μF, and 1000 μF for Sequence-1. During constant current region (CC-R) as indicated in C_{scan} = 100 μF, voltage across C_{in} remains stable i.e., ΔV_{Cin} is negligible. However, ΔV_{Cin} becomes significant during the slope region, and C_{scan} determines its rate. Consequently, ΔV_{Cin} = 3.34 V is highest for 100 μF and its magnitude starts reducing with higher capacitance. For instance, ΔV_{Cin} = 1.1 V and ΔV_{Cin} = 0.54 V occur with 470 μF and 1000 μF, respectively. Worth mentioning here that, the smoothness of P-V curve is not disturbed by ΔV_{Cin} as shown in P_{pv} graph of Fig. 8 (Sequence-1).

The matter is much complicated during Sequence-2 as C_{in} experiences second order transient at the start of scanning. This, in turn, produces swings in I-V curve, thus deteriorating the quality of I-V curve as shown in lower graphs of Fig. 8. It is because of the reason that C_{in} experiences the step change in current as I_{pv} of $0.9V_{oc}$ (before scanning) suddenly jumps to I_{sc} during scanning in Sequence-2. Such second order transient is also observed in parallel capacitor framework (Spertino et al., 2013). In case of C_{scan} = 100 μF, these effects are severe as shown in Fig. 8. However, the effects of these swings can be eliminated with the higher capacitance value (Spertino et al., 2015).

The optimum value of C_{scan} relies on the settling time (t_s) of transients. The second order transfer function of boost converter is indicated in (8), whose characteristics depend on C_{in} and L (Femia et al., 2005; Ortiz-Valencia and Ramos-Paja, 2015). In addition, natural frequency (ω_n) and damping ratio (ξ) of transient are expressed in (9) and (10) respectively (Femia et al., 2005; Ortiz-Valencia and Ramos-Paja, 2015):

$$\frac{v(s)}{d(s)} = -\frac{V_o}{C_{in}Ls^2 + \frac{L}{R_{mpp}}s + 1} \quad (8)$$

$$\omega_n = \sqrt{\frac{1}{C_{in}L}} \quad (9)$$

$$\xi = \frac{1}{2 \times R_{mpp}} \sqrt{\frac{L}{C_{in}}} \quad (10)$$

To evaluate settling time (t_s), the time (t_p) of first peak is required that can be estimated through (11):

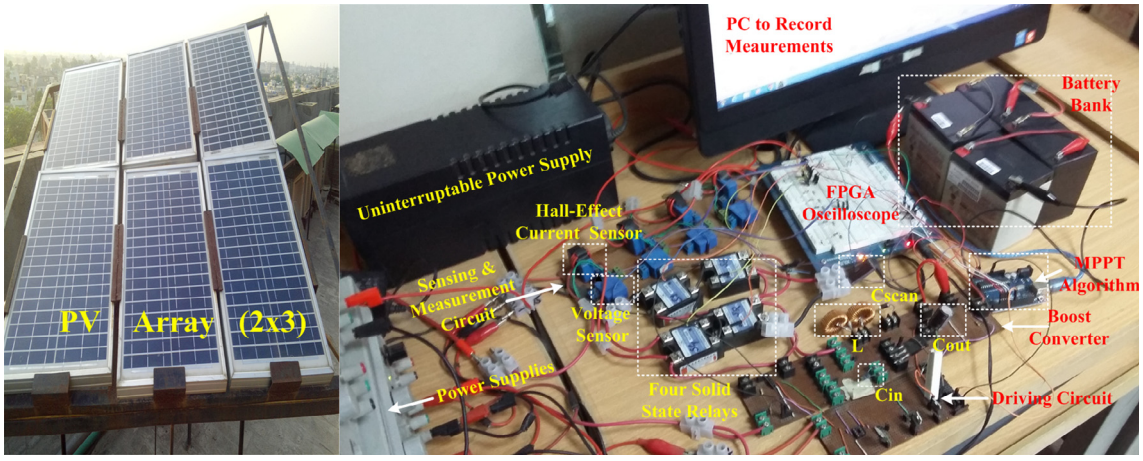

Fig. 7. Details of complete experimental test bench.

Table 1
Using C_{in} = 10 μF, tracings of I-V curves with distinct C_{scan} capacitors.

C_{in}	I_{sc}	V_{oc}	C_{scan}	Sequence-1 Tracing			Sequence-2 Tracing		
				Exp. (t_f)	Theor. (t_f)	Voltage drop (ΔV_{Cin})	First peak (V_{peak})	Exp. time of first peak (t_p)	Exp. transient's settling time (t_s)
10 μF	3.44 A	36.8 V	100 μF	2.41 ms	1.95 ms	3.34 V	12.48 V	0.19 ms	1.71 ms
	3.4 A	36.89 V	220 μF	4.78 ms	4.34 ms	2 V	14.48 V	0.19 ms	1.90 ms
	3.44 A	36.89 V	470 μF	9.15 ms	9.16 ms	1.1 V	13.02 V	0.20 ms	2.39 ms
	3.4 A	36.8 V	680 μF	14.52 ms	13.38 ms	0.72 V	13.48 V	0.20 ms	2.45 ms
	3.36 A	36.71 V	1000 μF	17.4 ms	19.86 ms	0.54 V	13.30 V	0.19 ms	2.30 ms
	3.4 A	36.62 V	2200 μF	39.36 ms	43.08 ms	0.28 V	11.92 V	0.19 ms	2.28 ms

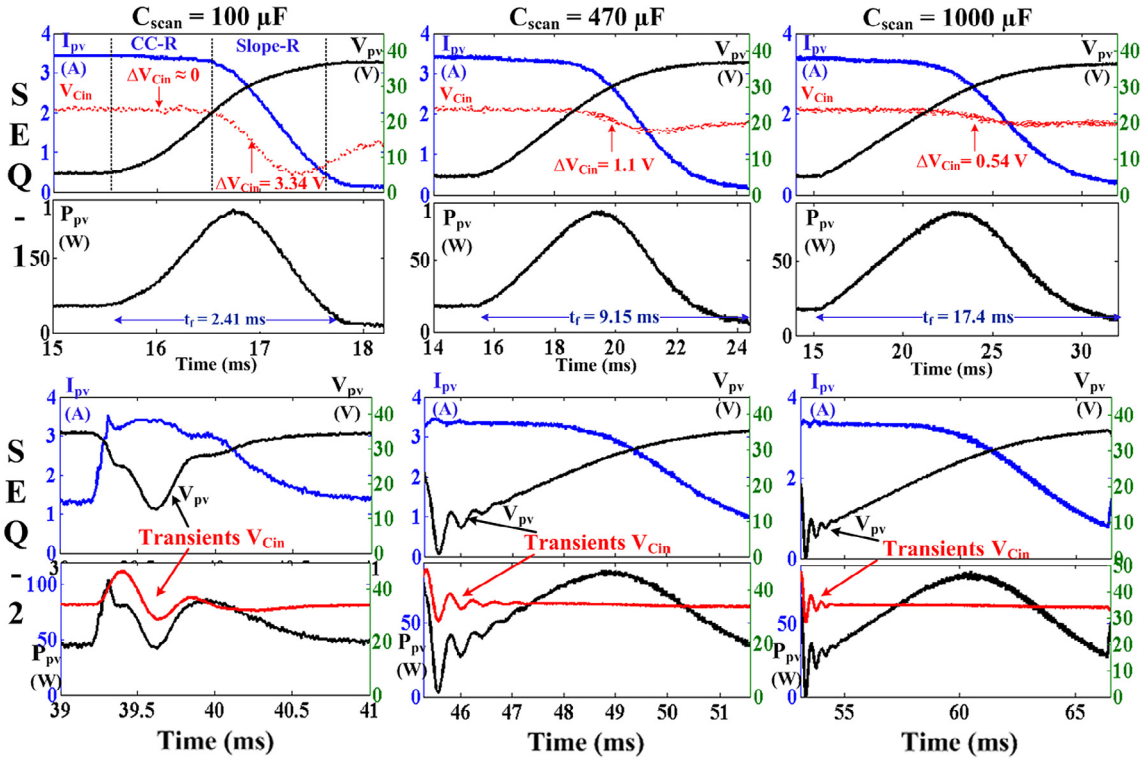

Fig. 8. Using C_{in} = 10 µF, scanning of I-V curves with distinct C_{scan} capacitors.

$$t_p = \frac{\pi}{\omega_n\sqrt{1-\xi^2}} \tag{11}$$

where R_{mpp} can be calculated from V_{mpp} and I_{mpp}. In present case of 2 × 3 array, V_{mpp} and I_{mpp} are 44 V and 3.63 A, respectively and C_{in} and L of converter are set at 10 µF and 424 µH, respectively. By putting the values of these parameters in above expressions, t_p = 0.22 ms is calculated from (11). This value is very close to average experimental value of t_p = 0.193 ms as observed from Sequence-2 of Table 1. Thereafter, the settling time (t_s) = 2.2 ms is estimated by multiplying t_p = 0.22 ms with a factor of 10. The value of t_s = 2.2 ms is similar to average experimental value of t_s = 2.17 ms as observed in Table 1. Finally, the transients are allowed to swing upto first 20% segment of I-V curve as MPP/GM does not appear in it; a factor of 5 is used to calculate the final time (t_f):

$$t_f = 5 \times t_s = 5 \times 10 \times t_p = 50 \times \frac{\pi}{\omega_n\sqrt{1-\xi^2}} \tag{12}$$

Expression (12) is set as a benchmark formula to calculate t_f. The value of which can be substituted in (6) to calculate C_{scan}. Like in the present case, t_f is calculated as 10.8 ms from (12). By putting this value in (6), C_{scan} is 490 µF. With C_{scan} = 470 µF (standard value close to 490 µF) second order transient remains within 20% during Seuence-2, while ΔV_{Cin} is inacceptable range of 1.1 V during Sequence-1 as shown in Fig. 8. The details of data are tabulated in Table 1. Note that for complete I-V curve sweep, Sequence-1 should be preferred as it is free from second order transient of converter.

Table 2 presents the case with C_{in} fifteen times greater than the capacitance calculated from (7). The higher C_{in} value doesn't produce any impact during Sequence-1 as tracings of I-V curve virtually remain the same. For instance, upper graphs of Fig. 9 (C_{in} = 150 µF) and Fig. 8 (C_{in} = 10 µF) show similar I-V curve tracings for C_{scan} = 470 µF and C_{scan} = 1000 µF. Also, ΔV_{Cin} values for same sets of C_{scan} capacitors are similar as confirmed from Tables 1 and 2.

The scenario is different during Sequence-2 as higher C_{in} reduces the peak voltage (V_{peak}) of the transient. It can be observed from Sequence-2 section in Table 2 that the average V_{peak} = 4 V with C_{in} = 150 µF is considerably reduced compared to average V_{peak} = 13 V with C_{in} = 10 µF. Thus, justifying the fact that peak magnitude is reduced with higher output capacitance. However, t_p = 0.795 ms (calculated from (11)) becomes large compared to t_p = 0.22 ms of C_{in} = 10 µF. The t_p = 0.795 ms is close to the average experimental value of t_p = 0.57 ms as shown in Sequence-2 of Table 2. Therefore settling time t_s = 7.95 ms (t_p × 10) shows good similarity to average experimental value of t_s = 5.4 ms. Using (12), t_f is equal to 39.75 ms, which is used to calculate C_{scan} = 1.803 mF from (6). Lower graph of Fig. 9 (Sequence-2) depicts that with C_{scan} = 1.820 mF, the second order transient remains within first

Table 2
Using C_{in} = 150 µF, tracings of I-V curves with distinct C_{scan} capacitors.

C_{in}	I_{sc}	V_{oc}	C_{scan}	Sequence-1 Tracing			Sequence-2 Tracing		
				Exp. (t_f)	Theor. (t_f)	Voltage drop (ΔV_{Cin})	First peak (V_{peak})	Exp. time of first peak (t_p)	Exp. transient's settling time (t_s)
150 µF	3.48 A	36.71 V	100 µF	2.9 ms	1.92 ms	3.34 V	4.06 V	0.54 ms	2.89 ms
	3.52 A	36.62 V	220 µF	4.5 ms	4.16 ms	2.18 V	3.96 V	0.53 ms	2.56 ms
	3.56 A	36.52 V	470 µF	8.5 ms	8.77 ms	1.28 V	3.70 V	0.57 ms	5.00 ms
	3.52 A	36.52 V	680 µF	13.4 ms	12.83 ms	0.9 V	4.16 V	0.61 ms	5.13 ms
	3.52 A	36.25 V	1000 µF	15.8 ms	18.72 ms	0.64 V	4.52 V	0.56 ms	5.40 ms
	3.48 A	36.52 V	1820 µF	33.9 ms	34.73 ms	0.32 V	4.08 V	0.58 ms	5.80 ms

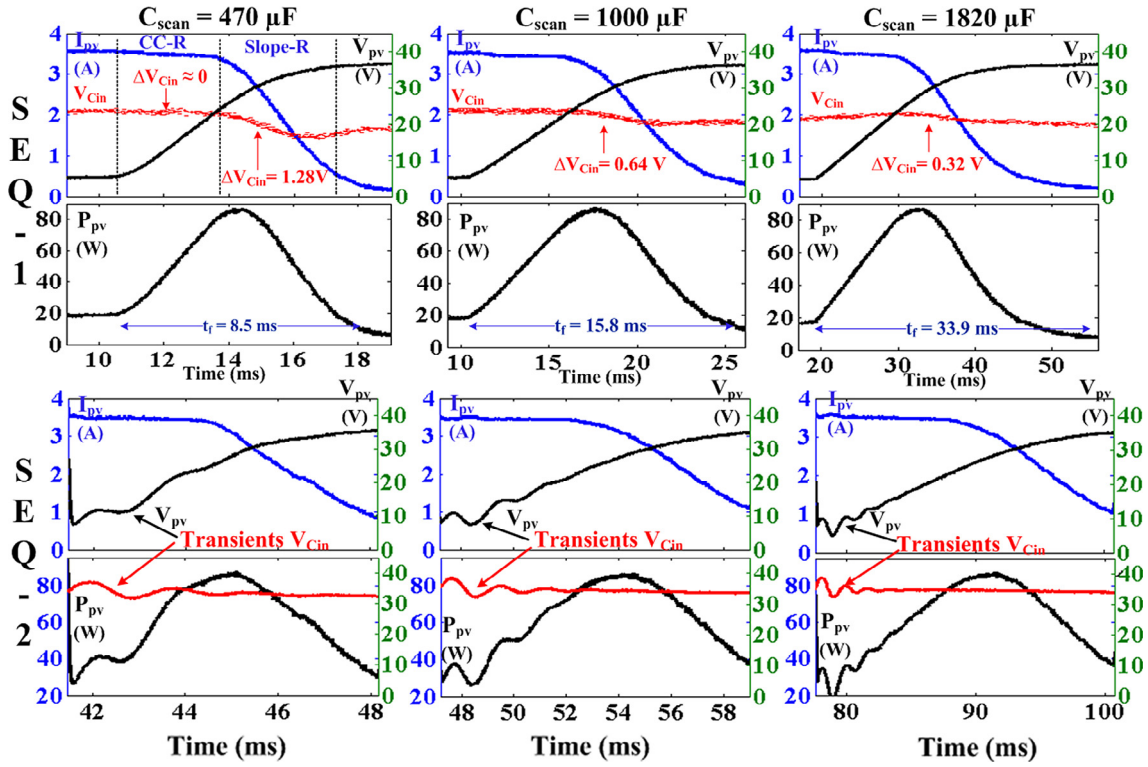

Fig. 9. Using C_{in} = 150 µF, scanning of I-V curves with distinct C_{scan} capacitors.

20% portion of I-V curve and I-V curve is smooth afterwards. Note that for a sufficient large C_{in} size i.e., 20 times higher than C_{in} of (7), V_{peak} of second-order transient approaches 0 V, thus C_{scan} of same size or double of C_{in} can be connected.

5. Simulation experiments & comparative analysis

For relative investigation, four techniques: proposed MPPT (C_{scan}), parallel capacitor based MPPT (C_{par}) (Spertino et al., 2015), restricted voltage window based MPPT (VWS) (Boztepe et al., 2014), and P&O are executed in Matlab/Simulink through comprehensive PV array model (Villalva et al., 2009). PV array consists of three modules in series, each of them belongs to type Kyocera-200GT. Battery load of 100 V is used and boost converter is employed between PV array and load. The converter components are rated as C_{in} = 250 µF, L = 250 µH and switching frequency f_{sw} = 15 kHz. The H-bridge setup shown in Fig. 3(a) is used to implement the proposed method. Concerning the hardware implementation of remaining three methods, the same circuit shown in Fig. 3(a) is employed and H-bridge is omitted. However, for the operation of C_{par} method (Spertino et al., 2015), an additional circuit shown in Fig. 1(a) with dotted lines is connected between PV array and converter. To trace the P-V curve, the proposed C_{scan} and C_{par} (Spertino et al., 2015) use a capacitor size of 450 µF. On the other hand, ΔD = 0.02 is used for P&O and VWS (Boztepe et al., 2014). The sampling rate of PV system is set at 10 ms.

To begin with, all techniques are permitted to settle at MPP under standard testing condition (STC) condition (condition-1) as depicted by region Q1 in Fig. 10(a). In the process, proposed C_{scan} scans the P-V curve in its Sequence-1 operation, and C_{scan} is charged upto $0.9V_{oc}$. After that, the operating points of MPPTs move from region Q1 to Q2 due to battery load, when PV array is partially shaded with condition-2 (P-V curve – three LMs) as appeared in Fig. 10(b). Fig. 11(a) presents the P_{pv} and V_{pv} of proposed C_{scan}, where the MPPT identifies the change in condition at

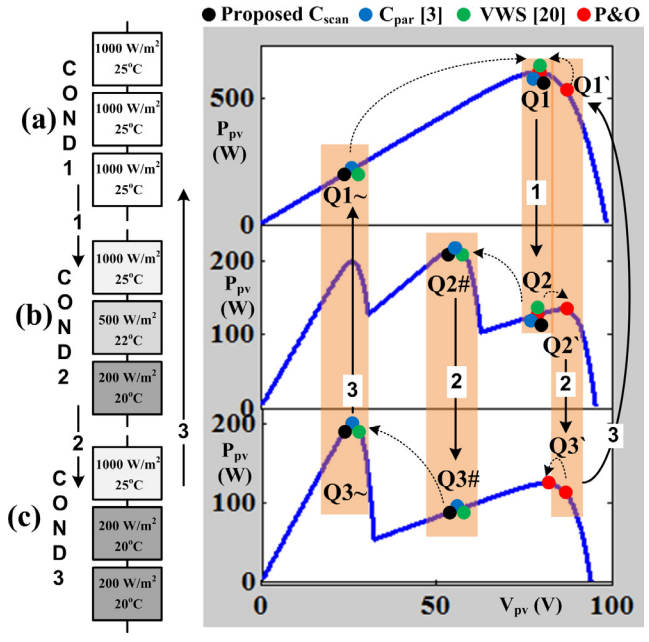

Fig. 10. PV array with different conditions, regions of MPPTs and MPP points.

20 ms; initiates the Sequence-2 (capacitor discharging sequence) by setting V_{pv} at $0.9V_{oc}$, and then scans the P-V curve for ≈10 ms (30–40 ms). During which, the C_{scan} method experiences three LMs, and filters the GM through peak detection algorithm. Finally, it settles the PV array at V_{mpp} of GM by modulating the D of converter. C_{par} (Spertino et al., 2015) (blue line) also initiates the process of scanning at 20 ms as shown in Fig. 11(b), and successfully operates the PV array at GM. However, no power is delivered to load during scanning of P-V curve. The resulting response of VWS (Boztepe et al., 2014) (green line) is shown in Fig. 12(b). It exami-

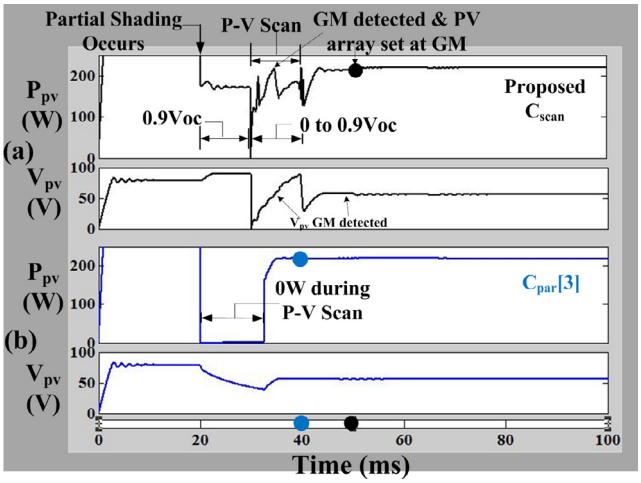

Fig. 11. P-V scanning of proposed C_{scan} and C_{par} MPPTs.

nes several samples to identify the GM vicinity, and then uses P&O to detect the GM precisely. The conventional P&O converges to LM as indicated in Fig. 12(a). With the exception of P&O, all other MPPTs successfully identified the GM. The detection time of GM/LM are: proposed C_{scan} = 40 ms, C_{par} (Spertino et al., 2015) = 30 ms, VWS (Boztepe et al., 2014) = 200 ms and P&O = 90 ms (LM). The dynamic response of these MPPTs can be evaluated from Fig. 12(c). Since the proposed C_{scan} consumes one sample to set PV array at $0.9V_{oc}$ prior to scan the P-V curve, C_{par} (Spertino et al., 2015) MPPT has the fastest response. Nevertheless, the proposed method outperforms every technique in terms of energy yield as it starts providing increased energy after 50 ms.

It can be seen from zoom-1 graph in Fig. 12(c), C_{par} (Spertino et al., 2015) method does not provide any energy during scanning (blue curve). This compromised the dynamic efficiency of the technique compared to proposed C_{scan} method. However, it provides more energy than VWS (Boztepe et al., 2014) (green curve) and P&O (red curve) after 70 ms and 80 ms, respectively as shown in zoom-2 graph. The deprived energy yield of VWS (Boztepe et al., 2014) algorithm is due to two reasons: (1) regulation of V_{pv} at different points of P-V curve is executed through second-order boost converter, which requires atleast 10 ms for each V_{pv} point, and (2) during GM search, the VWS (Boztepe et al., 2014) is not operated close to MPP. As a result, VWS (Boztepe et al., 2014) almost took 190 ms to provide more energy than P&O as indicated by arrow-3 in Fig. 12(c). Although P&O has caught in LM, it falls in vicinity of LM as shown in Fig. 10(b). Therefore, it requires less perturbations to reach there. Furthermore, the power deficit of LM is not immense compared to GM. This is the reason that unlike proposed C_{scan} and C_{par} (Spertino et al., 2015), VWS (Boztepe et al., 2014) takes ample time to yield better energy than P&O.

The shading pattern of PV array is changed from condition-2 (partial shading – three LMs) to condition-3 (partial shading – two LMs) as shown in Fig. 10(c). During previous condition, P&O caught in LM as mentioned by region Q2′ in Fig. 10(b), it moves to Q3′. Since other MPPTs operate in GM region i.e., Q2#, they fall in the same region Q3#. P&O nearly falls at LM and once again converges to it. The other three algorithms successfully tracked the GM. This time, the proposed MPPT executes the Sequence-1 (capacitor charging sequence). First, it sets the array at $0.1V_{oc}$ by adjusting D as shown in Fig. 13(a), when condition changes at 20 ms. After that, it scans the P-V curve from 0V to $0.9V_{oc}$ to detect the GM, and finally forces the array to operate at GM. Clearly, the proposed MPPT extracts more power from PV array, and starts providing increased energy after 60 ms compared to other MPPTs as illustrated in Fig. 13(c). The second best technique is C_{par} (Spertino et al., 2015) as it outperforms both VWS (Boztepe et al., 2014) and P&O at 70 ms indicated by Arrow-1. The weakest MPPT is VWS (Boztepe et al., 2014), which outperforms the P&O at 130 ms as indicated by Arrow-2 in Fig. 13(c). This time, LM in which P&O gets trapped has a considerable power deficit compared to GM as shown in Figs. 13(a) and 10(c); other MPPTs comprehensively outperform P&O.

Finally, the conditions are reverted back to STC i.e., all modules receive the same irradiance. Fig. 14(a) shows the response of proposed C_{scan} and P&O, while Fig. 14(b) displays the response of other two techniques. The effective performance of P&O can be evaluated from Fig. 10 that during the last condition, P&O operated at V_{pv} values in the region Q3′. As a result, it settles close to MPP region i.e. Q1′ and requires few samples to search the MPP. Other three MPPTs move from region Q3∼ to Q1∼, and therefore they settle in a region far away from the MPP vicinity. Even with such big advantage of P&O, it can be seen from Fig. 14(c) that the proposed MPPT outperforms P&O by a notable margin. While, the

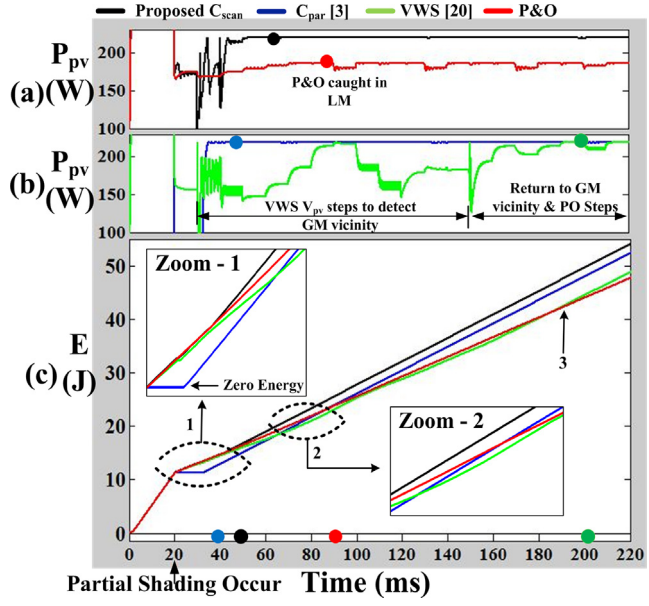

Fig. 12. Dynamic efficiencies of MPPTs under partially shaded PV array of condition-1.

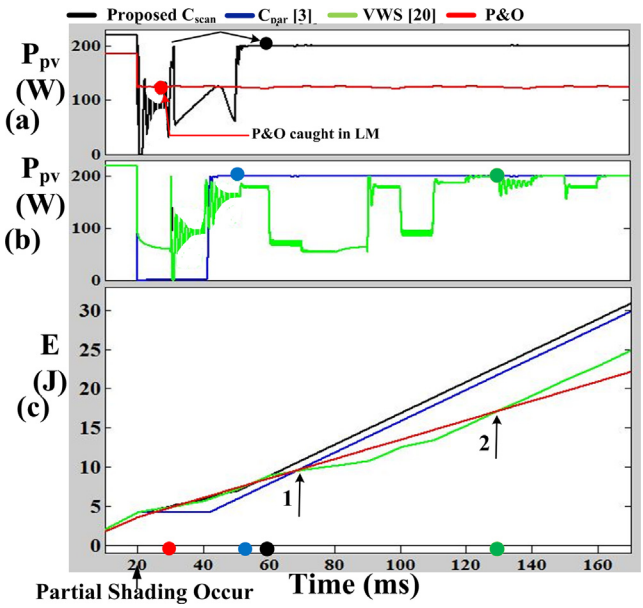

Fig. 13. Performances of MPPTs under partially shaded PV array of condition-2.

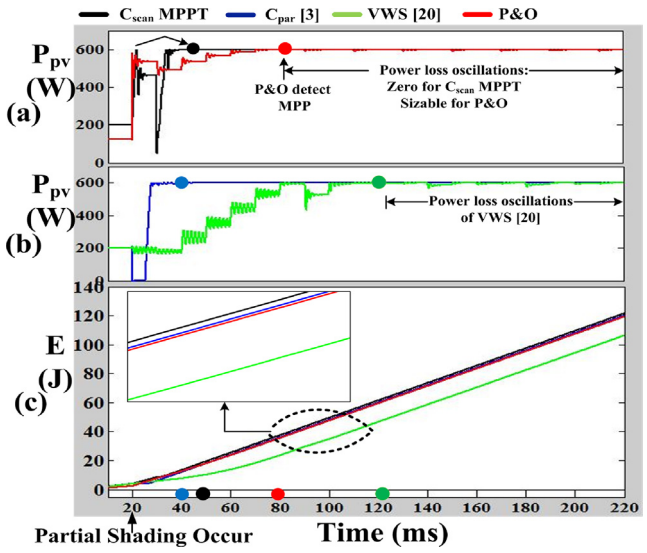

Fig. 14. Dynamic and steady efficiencies of MPPTs under uniformly irradiated PV array.

performance of C_{par} (Spertino et al., 2015) is close to P&O and VWS (Boztepe et al., 2014) is unable to yield more energy than P&O. Under present uniform STC condition, due to large overall current generated by the array the scanning duration for the proposed C_{scan} is nearly 6 ms, which is less compared to previous shading conditions. Furthermore, the proposed MPPT is immune to power loss oscillations around MPP under steady conditions as shown in Fig. 14(a). While, VWS (Boztepe et al., 2014) and P&O oscillate around MPP. This makes the C_{scan} operation highly efficient under steady weather conditions.

Table 3 summarizes the performance of techniques in terms of dynamic and steady state efficiencies. It can be evaluated from table that the proposed MPPT outperforms other MPPTs by a considerable margin. Furthermore, compared to C_{par} (Spertino et al., 2015), which requires three switches plus a dump load, the proposed MPPT requires four switches and no dump load. MPPTs VWS (Boztepe et al., 2014) and P&O do not require extra circuit, nevertheless the performance advantage of proposed MPPT will quickly recover the cost of extra switches.

6. Practical implementation and experimental results

6.1. Capacitor retention charge for Sequence-2

Under practical conditions, C_{scan} capacitor always loses its charge with time due to leakage phenomena. Therefore, C_{scan} with low ESR and high dielectric constant should be selected. Otherwise, it may prompt scanning issues during Sequence-2 if there is a considerable delay between the two sequences. To elaborate this matter, an electrolytic capacitor of 470 μF made of aluminum dielectric is selected. According to manufacturer's datasheet (https://www.melopero.com/datasheets/47uF.pdf), the leakage current (I_{leak}) after every two minutes can be determined from (13). Using I_{leak}, the holding charge of capacitor in terms of voltage (V_{hold}) can be calculated from (14):

$$I_{leak} = 0.01CV_{initial} \tag{13}$$

$$V_{hold} = V_{initial} - \frac{I_{leak}}{C} \tag{14}$$

Assuming C_{scan} is charged upto 35.42 V ($V_{initial}$), I_{leak} comes out to be 166.5 μA from (13) after two minutes. Using I_{leak}, the holding charge of C_{scan} can be found out from (14) as 35.07. This means 0.35 V loss of charge after two minutes i.e., 0.18 V per min. To

Table 3
Comparison of power efficiency between different MPPT methods.

Condition	Time Period (ms)	% Power Efficiency of MPPTs			
		Proposed C_{scan}	Parallel C_{par} (Spertino et al., 2015)	VWS Method (Boztepe et al., 2014)	P&O
Dynamic - 1	20–200	97.57	93.33	84.48	83.31
Dynamic - 2	20–160	89.18	85.76	66.58	62.09
Dynamic - 3	20–120	95.79	93.53	71.17	95.09
Steady	120–220	99.99	99.98	99.34	99.74

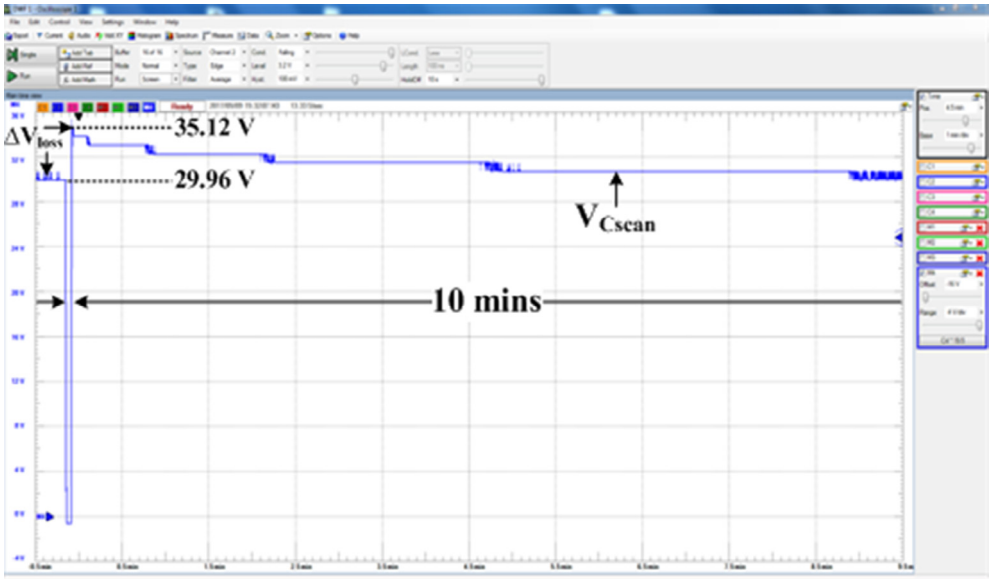

Fig. 15. Experiment of charge loss of C_{scan} capacitor with time.

verify this, an experiment has been performed where C_{scan} in initially charged upto ≈35.12 as shown in Fig. 15. After 10 min, the C_{scan} retains the charge upto 29.96 V i.e., 0.52 V per min. The value of 0.52 V shows resemblance to ideal value of 0.18 V as some of the charge is consumed by the measuring instrument. A good estimation can be 0.35 per minute. Therefore, after 10 min, C_{scan} will lose 3.5 V. This implies that during Sequence-2, the I-V curve is scanned from 3.5 V, instead of 0 V, which is still near to 0.1 V_{oc}. It is safe to assume that conditions will change every 10 mins. Moreover, 0.35 V/min loss in charge can be reduced further using high quality capacitor. However, if condition remains unchanged for more than 15 min, the technique can be re-started by discharging C_{scan} and then reinitialize the Sequence-1.

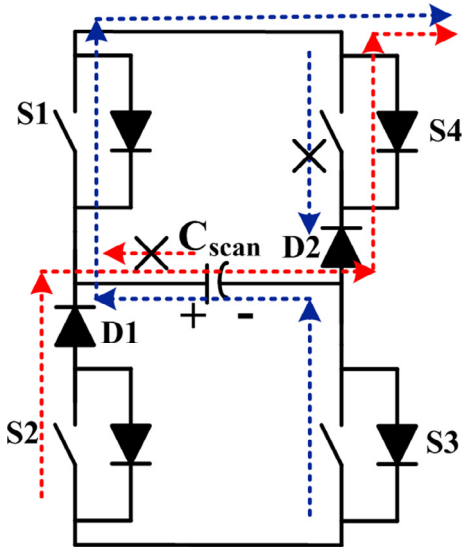

Fig. 16. Two diodes (D1 and D2) are connected to deal with bypass diodes of H-bride.

6.2. H-Bridge issues

Fig. 16 shows that each solid-state device of H-bridge contains a bypass diode. These diodes are connected across the devices for protection. To deal with bypass diodes and simultaneously enhancing the circuit stability and protection, two diodes (D1 and D2) are incorporated in the circuit as shown in Fig. 16. When S2 and S4 are switched on during Sequence-1, C_{scan} starts charging and current follows the path as depicted by red-line. The moment S2 is switched off and S3 is switched on, reverse current cannot flow as D1 blocks it. In addition, D1 gives the circuit stability that S2 and S3 can be toggled simultaneously. During Sequence-2 when S3 and S1 are switched on, C_{scan} is in discharging state as current follows the path as shown by blue-line in Fig. 16. It can be evaluated that without D2, current can flow through bypass diode of S4, eventually short-circuiting C_{scan}.

6.3. Experimental tests

Using the same experimental setup as mentioned in Section 4, experiments are performed with C_{in} = 10 μF and C_{scan} = 450 μF and sampling rate is set at 5 ms. C_{scan} is selected according to same criterion as explained in Section 4. Fig. 17 displays the tracings of

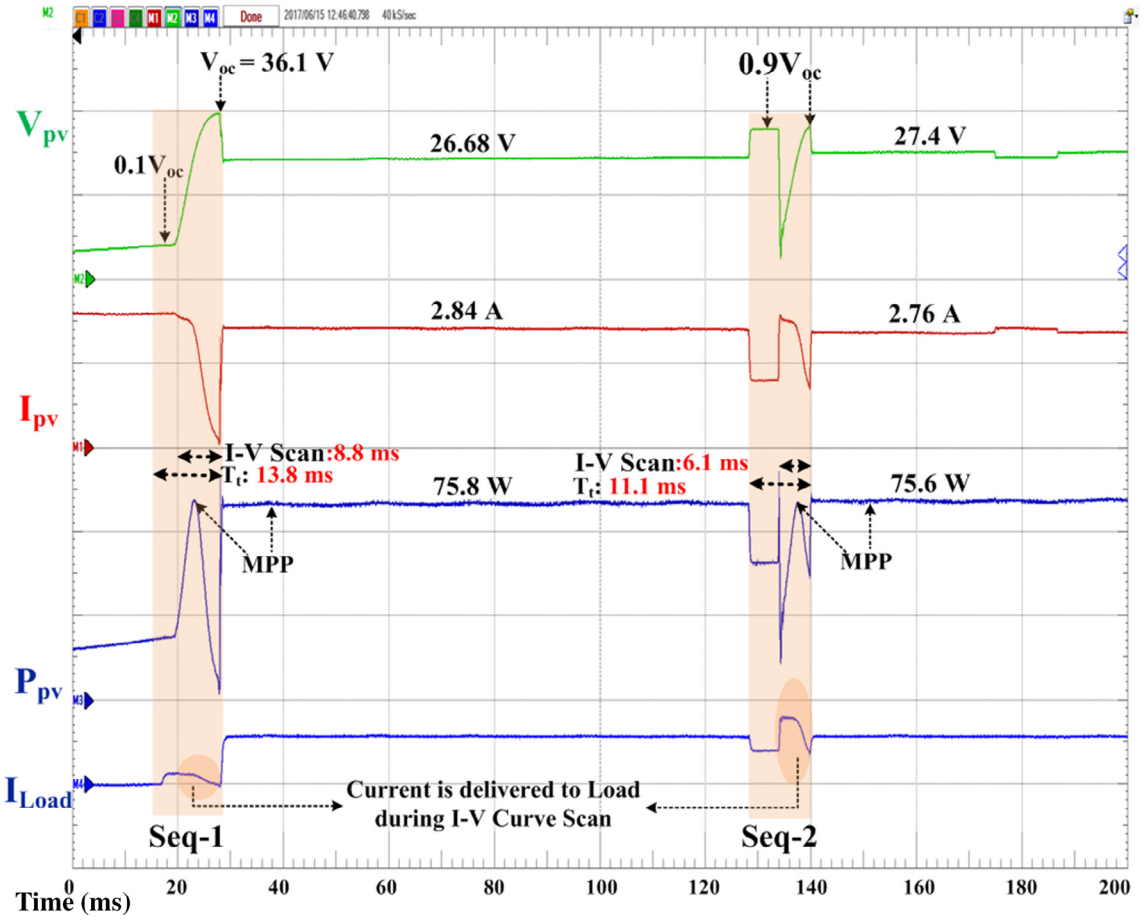

Fig. 17. I-V curve scanning of both sequences with I_{load}.

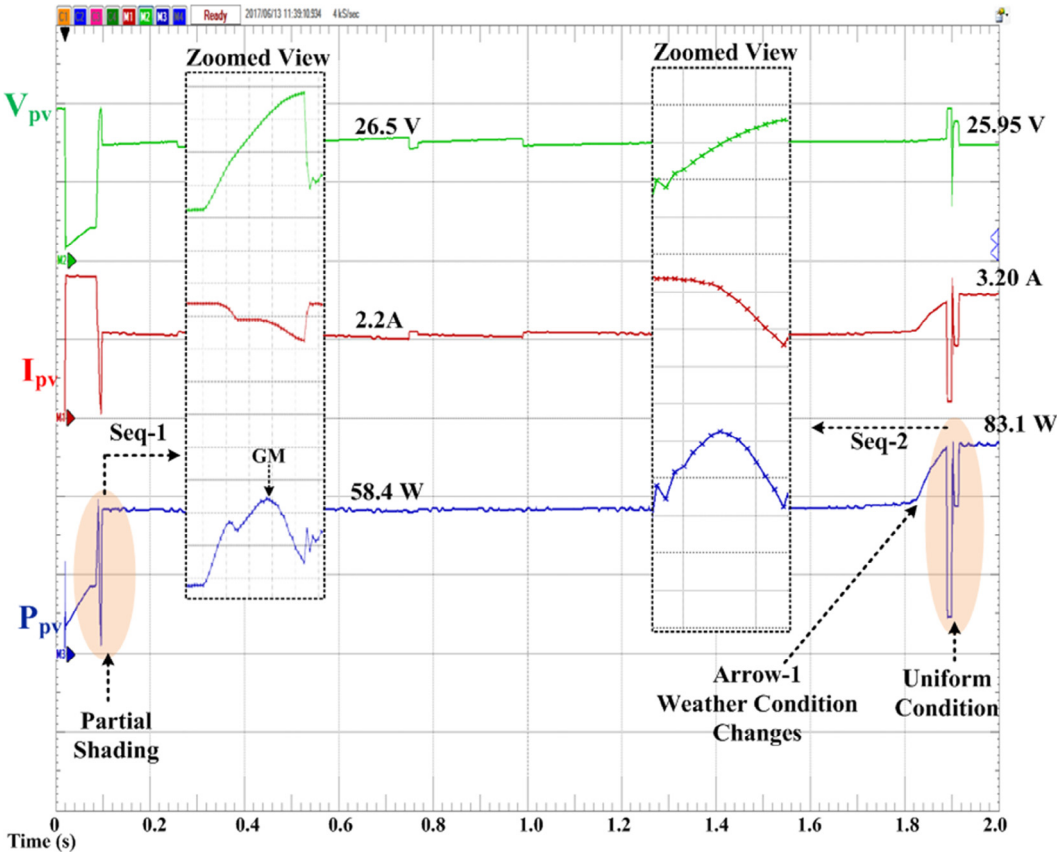

Fig. 18. Performance of proposed scheme with C_{in} = 10 μF and C_{scan} = 470 μF under partial and uniform conditions.

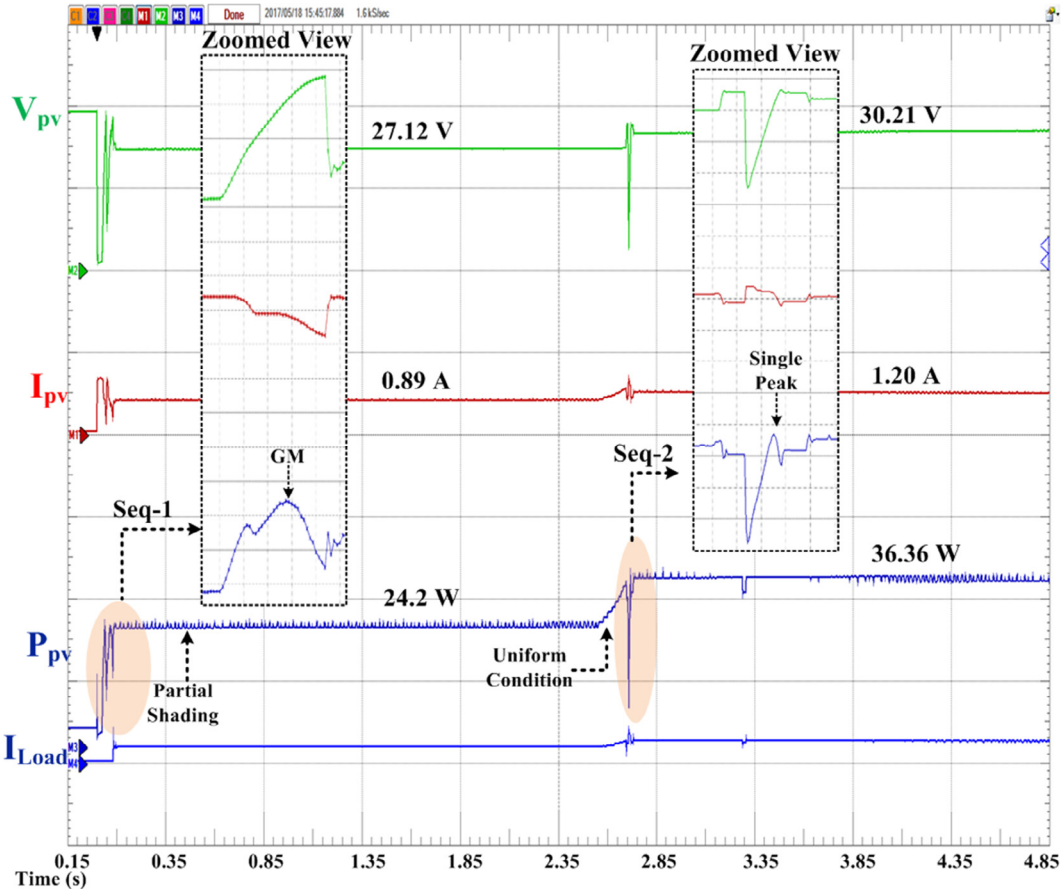

Fig. 19. Performance of proposed scheme with C_{in} = 150 μF and C_{scan} = 470 μF under partial and uniform conditions.

I-V curve for both sequences. The two tracings are deliberately scanned at a difference of 100 ms. Two technical aspects of proposed MPPT can be confirmed: (1) the scheme identifies the MPP points during both sequences and operates the PV array at those optimal points, and (2) current is delivered to load during scanning of I-V curve as highlighted in I_{load} line of Fig. 17.

A proper experiment is performed, in which PV array is partially shaded initially. It can be seen from Fig. 18 that proposed MPPT scans the I-V curve and identifies GM. After that, PV array is made un-shaded at Arrow-1. At this point, the power condition is violated, and Sequence-2 is revoked by the proposed MPPT. As a result of this, the proposed MPPT once again identifies MPP and successfully operates the PV array at MPP. Using the same settings, another experiment is performed with same $C_{scan} = 450\ \mu F$, but higher $C_{in} = 150\ \mu F$ is connected. Fig. 19 shows that on both occasions, proposed MPPT detects the optimal point. Although $C_{scan} = 1.8$ mF should be connected with $C_{in} = 150\ \mu F$, the experiment with $C_{scan} = 450\ \mu F$ is performed to indicate the behavior of proposed MPPT.

7. Concluding remarks

The investigation of I-V/P-V curves of PV array is an essential requirement for two main applications: (1) tracking of maximum power for un-shaded or partially shaded scenarios, and (2) parametric characterization of PV modules. Both these tasks can be performed in an inexpensive and uncomplicated way by utilizing the transient evolution of series capacitor. For MPP application, the scanning of P-V curve through single order capacitor provides considerable duration advantage compared to second order DC-DC converter. In this paper, a unique H-bridge architecture is being presented to scan the P-V curve through capacitor in series. The control algorithm of the proposed method works in two sequences. The sizing criterion of scanning capacitor is comprehensively discussed with regard to array size and input capacitor of converter. It has been proved through simulation studies that the proposed MPPT has outperformed the previous MPPTs by a significant margin. The proposed MPPT gained advantage over the parallel capacitor MPPT because it neither separated the array from load nor dumped the energy stored in capacitor through an extra resistor. Finally, the fundamental operation of proposed MPPT has been verified through experimental results.

References

Accessed Online, 2017. <https://www.melopero.com/datasheets/47uF.pdf>.

Ahmed, J., Salam, Z., 2014. A maximum power point tracking (MPPT) for PV system using Cuckoo Search with partial shading capability. Appl. Energy 119, 118–130.

Bekker, B., Beukes, H.J., 2004. Finding an optimal PV panel maximum and power point tracking method. IEEE AFRICON, 1125–1130.

Bidram, A., Davoudi, A., Balog, R.S., 2012. Control and circuit techniques to mitigate partial shading effects in photovoltaic arrays. IEEE J. Photovolt. 2 (4), 532–546.

Bizon, N., 2016. Global extremum seeking control of the power generated by a photovoltaic array under partially shaded conditions. Energy Convers. Manage. 109, 71–85.

Boztepe, M., Guinjoan, F., Velasco-Quesada, G., Silvestre, S., Chouder, A., Karatepe, E., 2014. Global MPPT scheme for photovoltaic string inverters based on restricted voltage window search algorithm. IEEE Trans. Power Electron. 61 (7), 3302–3312.

Chao, K.-H., 2014. An extension theory-based maximum power tracker using a particle swarm optimization algorithm. Energy Convers. Manage. 86, 435–442.

Chen, Y.T., Jhang, Y.C., Liang, R.H., 2016. A fuzzy-logic based auto-scaling variable step-size MPPT method for PV systems. Sol. Energy 126, 53–63.

Femia, N., Petrone, G., Spagnuolo, G., Vitelli, M., 2005. Optimization of perturb and observe maximum power point tracking method. IEEE Trans. Power Electron. 20 (4), 963–973.

González, J.M., Domínguez, J.A., Ruiz, J.M., Alonso, C., 2016. Ultracapacitors utilization to improve the efficiency of photovoltaic installations. Sol. Energy 134, 484–493.

Kotti, R., Shireen, W., 2013. Fast converging MPPT control of photovoltaic systems under partial shading conditions. In: IEEE International Conference on Power Electronics, Drives and Energy Systems (PEDES).

Kotti, R., Shireen, W., 2015. Efficient MPPT control for PV systems adaptive to fast changing irradiation and partial shading conditions. Sol. Energy 114, 397–407.

Kouchaki, A., Iman-Eini, H., Asaei, B., 2013. A new maximum power point tracking strategy for PV arrays under uniform and non-uniform insolation conditions. Sol. Energy 91, 221–232.

Liu, Fangrui, Duan, Shanxu, Liu, Fei, Liu, Bangyin, Kang, Yong, 2008. A variable step size INC MPPT method for PV systems. IEEE Trans. Ind. Electron. 55 (7), 2622–2628.

Mahmoud, M.M., 2006. Transient analysis of a PV power generator charging a capacitor for measurement of the I-V characteristics. Renew. Energy 31 (13), 2198–2206.

Mohanty, S., Subudhi, B., Member, S., Ray, P.K., 2015. A new MPPT design using grey wolf optimization technique for photovoltaic system under partial shading conditions. IEEE Trans. Sustain. Energy, 1–8.

Moradi, M.H., Reisi, A.R., 2011. A hybrid maximum power point tracking method for photovoltaic systems. Sol. Energy 85 (11), 2965–2976.

Munoz, J.V., Nofuentes, G., Aguilera, J., Fuentes, M., Vidal, P.G., 2011. Procedure to carry out quality checks in photovoltaic grid-connected systems: six cases of study. Appl. Energy 88 (8), 2863–2870.

Murtaza, A., Chiaberge, M., De Giuseppe, M., Boero, D., 2014a. A duty cycle optimization based hybrid maximum power point tracking technique for photovoltaic systems. Int. J. Electr. Power Energy Syst. 59, 141–154.

Murtaza, A., Chiaberge, M., Spertino, F., Boero, D., De Giuseppe, M., 2014b. A maximum power point tracking technique based on bypass diode mechanism for PV arrays under partial shading. Energy Build. 73, 13–25.

Ortiz-Valencia, P., Ramos-Paja, C., 2015. Sliding-Mode controller for maximum power point tracking in grid-connected photovoltaic systems. Energies 8 (11), 12363–12387.

Parlak, K.S., 2014. FPGA based new MPPT (maximum power point tracking) method for PV (photovoltaic) array system operating partially shaded conditions. Energy 68, 399–410.

Patel, H., Agarwal, V., 2008. Maximum power point tracking scheme for PV systems operating under partially shaded conditions. IEEE Trans. Ind. Electron. 55 (4), 1689–1698.

Petrone, G., Spagnuolo, G., Teodorescu, R., Veerachary, M., Vitelli, M., 2008. Reliability issues in photovoltaic power processing systems. IEEE Trans. Ind. Electron. 55 (7), 2569–2580.

Piegari, L., Rizzo, R., 2009. Adaptive perturb and observe algorithm for photovoltaic maximum power point tracking. IET Renew. Power Gener. 4 (January 2009), 317.

Punitha, K., Devaraj, D., Sakthivel, S., 2013. Artificial neural network based modified incremental conductance algorithm for maximum power point tracking in photovoltaic system under partial shading conditions. Energy 62, 330–340.

Seyedmahmoudian, M., Rahmani, R., Mekhilef, S., Oo, A. Maung Than, Stojcevski, A., Soon, T.K., Ghandhari, A.S., 2015. Simulation and hardware implementation of new maximum power point tracking technique for partially shaded PV system using hybrid DEPSO method. IEEE Trans. Sustain. Energy 6 (3), 850–862.

Sher, H.A., Murtaza, A.F., Noman, A., Addoweesh, K.E., Al-Haddad, K., Chiaberge, M., 2015. A new sensorless hybrid MPPT algorithm based on fractional short-circuit current measurement and P&O MPPT. IEEE Trans. Sustain. Energy 6 (4), 1426–1434.

Spertino, F., Sumaili, J., Andrei, H., Chicco, G., 2013. PV module parameter characterization from the transient charge of an external capacitor. IEEE J. Photovolt. 3 (4), 1325–1333.

Spertino, F., Ahmad, J., Ciocia, A., Di Leo, P., Murtaza, A.F., Chiaberge, M., 2015. Capacitor charging method for I-V curve tracer and MPPT in photovoltaic systems. Sol. Energy 119, 461–473.

Standard IEC 62446, 2009. Grid connected photovoltaic systems-minimum requirements for system documentation, commissioning test and inspection.

Subudhi, B., Pradhan, R., 2013. A comparative study on maximum power point tracking techniques for photovoltaic power systems. IEEE Trans. Sustain. Energy 4 (1), 89–98.

Villalva, M.G., Gazoli, J.R., Filho, E.R., 2009. Comprehensive approach to modeling and simulation of photovoltaic arrays. IEEE Trans. Power Electron. 24 (5), 1198–1208.

Wang, Y., Liu, Y., Wang, C., Li, Z., Sheng, X., Lee, H.G., Chang, N., Yang, H., 2016. Storage-less and converter-less photovoltaic energy harvesting with maximum power point tracking for internet of things. IEEE Trans. Comput. Des. Integr. Circuits Syst. 35 (2), 173–186.

Xiao, W., Ozog, N., Dunford, W.E., 2007. Topology study of photovoltaic interface for maximum power point tracking. IEEE Trans. Ind. Electron. 54 (3), 1696–1704.